Gyrotaxis in a Steady Vortical Flow

William M. Durham,[1] Eric Climent,[2] and Roman Stocker[1]

[1]*Department of Civil and Environmental Engineering, Massachusetts Institute of Technology, 77 Massachusetts Avenue, Cambridge, Massachusetts 02139, USA*

[2]*Institut de Mécanique des Fluides, Université de Toulouse, INPT-UPS-CNRS, Allée du Professeur Camille Soula, F-31400 Toulouse, France*

(Received 24 August 2010; published 6 June 2011)

We show that gyrotactic motility within a steady vortical flow leads to tightly clustered aggregations of microorganisms. Two dimensionless numbers, characterizing the relative swimming speed and stability against overturning by vorticity, govern the coupling between motility and flow. Exploration of parameter space reveals a striking array of patchiness regimes. Aggregations are found to form within a few overturning time scales, suggesting that vortical flows might be capable of efficiently separating species with different motility characteristics.

DOI: 10.1103/PhysRevLett.106.238102 PACS numbers: 47.63.Gd, 87.18.Hf, 87.85.gf, 92.20.jf

Spatial heterogeneity, or "patchiness," in the distribution of organisms affects important ecological processes, including competition, predation, the spread of epidemics, and the maintenance of species diversity [1]. We report on a biophysical mechanism that rapidly generates small-scale patchiness in the distribution of microorganisms and might have implications for marine phytoplankton. These unicellular, photosynthetic organisms are responsible for half of the world's oxygen production and represent the base of the oceans' food web. Patchiness in the distribution of phytoplankton is strongly coupled to ecosystem productivity [2] and has been found to extend down to centimeter scale [3–6].

Active locomotion is used by many organisms to achieve and maintain advantageous positions with respect to resources, predators, and each other, thereby conferring enhanced fitness. Although many marine microorganisms are motile, their motility is often neglected because swimming speeds are typically smaller than ambient flow speeds. Using a well-established flow model, we show that a coupling between motility and vortical fluid motion can drive aggregations of gyrotactic cells, with a rich diversity of steady-state cell distributions.

Motile phytoplankton often swim in a preferred direction $\mathbf{k}$ (typically vertical, to perform daily migration through the water column), owing to a stabilizing torque that can arise from an asymmetry in shape or body density, or the ability to sense the direction of gravity [7]. In moving fluids, cells further experience rotation due to gradients in velocity and cells are said to be gyrotactic [Fig. 1(a)]. Modeling cells as prolate ellipsoids, their swimming direction $\mathbf{p}$ is governed by [8]

$$\frac{d\mathbf{p}}{dt^*} = \frac{1}{2B}[\mathbf{k} - (\mathbf{k}\cdot\mathbf{p})\mathbf{p}] + \frac{1}{2}\boldsymbol{\omega}^* \times \mathbf{p} + \alpha\mathbf{p}\cdot\mathbf{E}^*\cdot[\mathbf{I} - \mathbf{pp}]. \quad (1)$$

Starred quantities indicate dimensional variables: $\boldsymbol{\omega}^*$ is the vorticity, $\mathbf{E}^*$ is the rate of strain tensor, $\mathbf{I}$ is the identity matrix, t^* is time, B is the characteristic time a perturbed cell takes to return to orientation $\mathbf{k}$ if $\boldsymbol{\omega}^* = 0$, and $\alpha = (\gamma^2 - 1)/(\gamma^2 + 1)$, where γ is the ratio of the cell's major to minor axes. When there is no preferred swimming direction ($B^{-1} = 0$) Jeffery orbits are recovered. Equation (1) applies to organisms much smaller than the scale of ambient velocity gradients, which allows cells to be modeled as point particles.

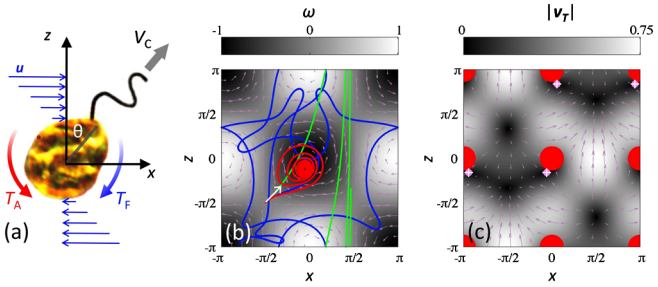

FIG. 1 (color online). (a) Gyrotactic microorganisms, such as the toxic marine phytoplankton *Heterosigma akashiwo* shown here (diameter ≈ 14 μm), swim in a direction, θ, set by a balance of torques. The torque due to flow (T_F) tends to rotate the cell, whereas the torque due to cell asymmetry (T_A)—for example bottom heaviness—tends to restore the cell to its preferential orientation, $\mathbf{k}$. V_C is the swimming speed. (b) Three cells, with different Ψ and Φ, initialized at the same location and orientation ($x = z = -\pi/2$; $\theta = \pi/4$; white arrow) in a TGV flow follow very different trajectories. $(\Psi, \Phi) = (0.1, 20)$ [light gray (green)], $(1, 0.2)$ [medium gray (red)], $(100, 0.5)$ [dark gray (blue)]. The TGV velocity and vorticity fields are shown by arrows and by shading, respectively. The domain is doubly periodic. (c) The most intense cell accumulation occurs when cells converge to equilibrium points, where total cell velocity $\boldsymbol{V}_T = (dx/dt, dz/dt) = (0, 0)$. Shown here is the "equilibrium double" regime ($\Psi = 1.1$, $\Phi = 0.25$). White crosses are numerical predictions of the equilibria, small pink circles are analytical results. Arrows and shading show $\boldsymbol{V}_T$ and $|V_T|$, respectively, assuming cell orientation is static. Large red circles denote regions where vorticity can overturn cells ($\omega\Psi > 1$).

The study of particle motion in vortical flows has a rich history, partly due to its importance in marine [9] and atmospheric [10] processes; the Taylor-Green vortex (TGV) flow [11] has been widely used, largely because of its tractability. The TGV flow is a two-dimensional array of steady, counterrotating vortices [Fig. 1(b)], with spacing L and maximum vorticity ω_o at the center of vortices. The nondimensional velocity $\mathbf{u} = [u, 0, w]$ and vorticity $\boldsymbol{\omega} = [0, \omega, 0]$ are $u = -\frac{1}{2}\cos x \sin z$, $w = \frac{1}{2}\sin x \cos z$, and $\omega = -\cos x \cos z$, where lengths, velocities, and vorticity are nondimensionalized by $1/m$, ω_o/m, and ω_o, respectively, and $m = 2\pi/L$.

To determine how of gyrotactic cells respond to vortical flows, we computed the trajectories of individual organisms swimming at constant speed V_C within a TGV flow. The nondimensional equations of motion for a cell are then

$$\frac{d\mathbf{p}}{dt} = \frac{1}{2\Psi}[\mathbf{k} - (\mathbf{k}\cdot\mathbf{p})\mathbf{p}] + \frac{1}{2}\boldsymbol{\omega}(\mathbf{X}) \times \mathbf{p} + \alpha\mathbf{p}\cdot\mathbf{E}(\mathbf{X})\cdot[\mathbf{I} - \mathbf{pp}], \quad (2)$$

$$\frac{d\mathbf{X}}{dt} = \Phi\mathbf{p} + \mathbf{u}(\mathbf{X}), \quad (3)$$

where $\mathbf{X} = [x, y, z]$, $\Psi = B\omega_o$, $\Phi = V_C m/\omega_o$, and time was nondimensionalized by $1/\omega_o$. We neglected the effect of cells on flow.

We first considered spherical cells ($\alpha = 0$) swimming within a vertical plane (x-z), for which Eq. (2) becomes $d\theta/dt = -\frac{1}{2}(\cos x \cos z + \sin\theta/\Psi)$ [12], where θ is the swimming direction relative to the vertical [Fig. 1(a)]. With these assumptions, the two parameters, Φ and Ψ, fully control the fate of the cells. Φ measures the swimming speed relative to the flow speed and Ψ is a measure of orientational stability; if $\omega\Psi > 1$ the cell can be overturned by vorticity [7] [large red circles, Fig. 1(c)].

We find that the spatial distribution of gyrotactic cells in vortical flow is highly dependent upon Ψ and Φ. We begin by comparing trajectories of three cells with different Ψ and Φ parameters, all initialized with the same orientation and position [Fig. 1(b)]. The slow, intermediately stable red cell ($\Phi = 0.2$, $\Psi = 1$) spirals inwards towards a single point, the fast and stable green cell ($\Phi = 20$, $\Psi = 0.1$) rapidly finds an upward path, whereas the slow and unstable blue cell ($\Phi = 0.5$, $\Psi = 100$) wanders aimlessly. These strikingly different behaviors highlight the complex interaction between motility and flow and suggest the existence of multiple regimes of phytoplankton aggregation in vortical flows.

A systematic exploration of Φ-Ψ parameter space revealed 10 distinct, time-invariant patchiness regimes (Fig. 2; at $t = 2000$). The strongest aggregation occurs when all cells converge to points where the equilibrium cell orientation is such that motility exactly balances flow [$d\theta/dt = dx/dt = dz/dt = 0$; Figs. 1(c), 2(b), and 2(c); movie 1 in [13]]. This can occur at either a single point [$x = \pi/2$, $z = \cos^{-1}(-2\Phi)$; Fig. 2(b)] or two points [$x = \cos^{-1}(\pm\Gamma^{1/2})$, $z = \tan^{-1}(-2\Psi\Phi)$, $\Gamma = (16\Psi^2\Phi^4 + 4\Phi^2 - 1)/(4\Psi^2\Phi^2 - 1)$; Figs. 1(c) and 2(c)] within each vortex.

Gyrotactic cells are known to collect in downwelling regions ($w < 0$) [12], a mechanism that was suggested to produce accumulation in turbulent flows [14]. We recover accumulation in downwelling regions in the "vertical migrator" regime [Fig. 2(d)], in which cells focus into vertical bands between vortices and swim upwards ($x = \pm\pi/2$, $\theta = 0$; movie 2 in [13]). Though these cells

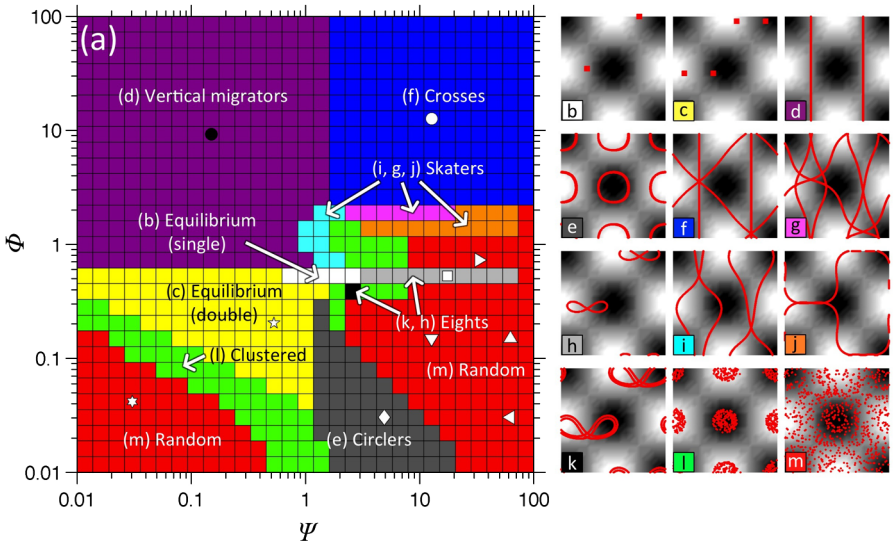

FIG. 2 (color online). (a) Parameter space of gyrotactic swimming in TGV flow, showing different patchiness regimes. Each square represents one of 900 simulations. In each simulation the trajectories of 400 randomly initialized cells were integrated until $t = 2000$. Ten distinct patterns emerge (b)–(k), not including the cases in which accumulation does not occur (m) or has not converged (l). For the "equilibrium" regimes (b),(c), all cells reside at the equilibrium points. The symbols in (a) correspond to (Ψ, Φ) values that are analyzed in Fig. 4(b) to investigate the role of cell elongation.

traverse both upwelling and downwelling regions, convergence prevails because cells spend more time in regions where swimming and flow oppose one another.

In contrast with earlier predictions [14], accumulation in downwelling regions is only one of many possible patterns of aggregation: a multitude of patterns arise in Φ-Ψ parameter space (Fig. 2). Unstable cells ($\Psi > 1$) are more susceptible to being rotated by vorticity. Slow unstable cells ($\Phi < 0.3$) are unable to escape vortices, leading to closed trajectories [Fig. 2(e); movie 3 in [13]). In contrast, fast unstable cells ($\Phi > 0.3$) are locally reoriented by vorticity, but can escape from vortices. They weave from one vortex to the other, producing diverse patterns [Figs. 2(g), 2(i), and 2(j); movie 4 in [13]), including some peculiar figure eights [Figs. 2(h) and 2(k)]. Finally, very fast unstable cells ($\Phi > 2$) have little time to be deflected by vorticity and can move diagonally in addition to vertically upwards [Fig. 2(f)]. Although for slow swimmers ($\Phi < 1$) there exist regimes where accumulation patterns did not emerge [Fig. 2(m)] or converge [Fig. 2(l)] by $t = 2000$, the diversity of accumulation patterns and their occurrence over a wide range of parameter space indicate that strong patchiness of gyrotactic cells is the norm within vortical flows, rather than the exception.

In addition to producing patchiness, vortical flow can stifle vertical migration. This effect can be quantified using the vertical migration rate, $W = \langle dz/dt \rangle / \Phi$, defined as the net upward speed of a cell averaged over all cells and over time ($t = 0$–10), normalized by Φ [Fig. 3(c)]. The upward movement of stable cells ($\Psi < 1$) is largely unaffected by flow ($W \sim 1$). In contrast, vertical migration of unstable cells ($\Psi > 1$) is severely impeded ($W \ll 1$), showing that vortical flow can trap gyrotactic cells at depth. The suppression of vertical migration is in line with simulations utilizing more complex flow fields [15].

To quantify patchiness, we partitioned the domain into a 15×15 grid of boxes and computed the box occupancy function, $f(n)$ [16], where n is the number of cells in a box (with mean λ). As cells accumulate in some boxes and leave others empty, the standard deviation of $f(n)$, σ, increases relative to its initial (Poisson) value, σ_P ($= \lambda^{1/2}$).

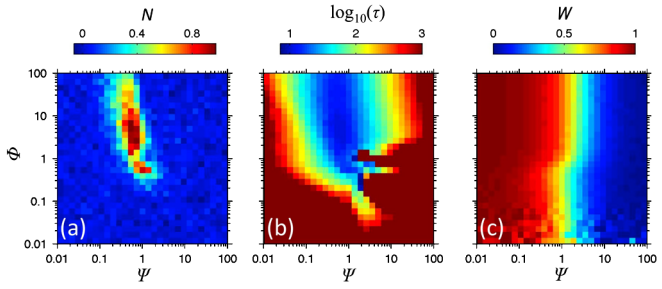

FIG. 3 (color online). (a) The degree of patchiness at time $t = 10$, quantified by the accumulation index N. $N > 0$ indicates aggregation. (b) The time, τ, required for cells to reach a time-invariant spatial pattern. (c) The normalized vertical migration rate W.

Thus, the accumulation index $N = (\sigma - \sigma_P)/\lambda$ is a measure of patchiness [16]. Figure 3(a) shows N in Φ-Ψ space at $t = 10$. Cells with motility faster than the flow ($\Phi > 0.5$) and intermediate stability ($\Psi \sim 1$) exhibit marked patchiness by $t = 10$; hence, accumulation by this mechanism can be rapid (within a few vortex time scales). Cells that accumulate the most swiftly belong primarily to the "vertical migrator," "equilibrium," and "skater" regimes (Fig. 2). This is also observed by computing the time τ required for a randomly distributed population to reach a time-invariant spatial distribution. The latter was calculated by fitting $N(t)$ with the exponential $\kappa\ (1 - e^{-t/\tau})$, where κ is a constant. The same region of parameter space ($\Phi > 0.5$, $\Psi \sim 1$) exhibits the fastest accumulation [Fig. 3(b)]. This result is readily rationalized: to accumulate, cells must swim across streamlines. Fast swimmers are able to make significant progress across streamlines, while intermediate stability represents a trade-off between persistent tumbling ($\Psi \gg 1$), which negates directed swimming, and excessive stability ($\Psi \ll 1$), which prevents cell orientation from being perturbed by the flow.

These findings assume that the fluid vorticity is orthogonal to the preferred swimming direction $\mathbf{k}$. To determine the effect of vortex orientation, we performed 3D simulations for spherical cells ($\alpha = 0$) by extruding the TGV flow in the $\mathbf{y}$ direction and allowing $\mathbf{k}$ to assume any orientation, prescribed by polar and azimuthal angles (η, β). The swimming direction was computed using Eqs. (2) and (3). When $\mathbf{k} = \mathbf{z}$ ($\eta = \beta = 0$), the x-z projection of the 3D time-invariant cell distribution is identical to the 2D simulation. As one varies $\mathbf{k}$, additional patchiness regimes emerge. Patchiness occurs over all orientations of $\mathbf{k}$, with the exception of a small region about $\mathbf{k} = \mathbf{y}$ [$\eta = \beta = \pi/2$; Fig. 4(a)], where cell orientation is unaffected by flow ($\boldsymbol{\omega} \times \mathbf{k} \approx 0$). Thus, the proposed patch generation mechanism is robust in 3D space.

Phytoplankton morphology is highly diverse: many species have nonspherical cell bodies or flagella that alter their

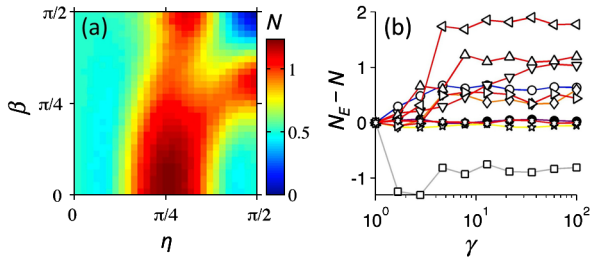

FIG. 4 (color online). (a) Gyrotactic cells form aggregations for almost any vortex orientation. Plotted here is the accumulation index N, at $t = 10$ and $\Phi = \Psi = 1$, as a function of the polar and azimuthal angles, η and β. (b) Cell elongation (aspect ratio $\gamma > 1$) produces an increase in patchiness in most regimes, compared to the case of spherical cells ($\gamma = 1$). Shown is the change in the accumulation index, $N_E - N$, due to elongation, at $t = 2000$. Symbols correspond to Φ, Ψ values and in Fig. 2(a). Representative cell distributions can be found in Fig. S1 in [13].

effective eccentricity. Elongated swimming particles in TGV flow, in the absence of a preferential swimming direction ($\Psi = \infty$), have been shown to aggregate along flow separatrices [17]. We determined how elongation influences the aggregation of gyrotactic cells for 10 values of Ψ and Φ [Fig. 2(a), symbols], for each of them varying the cell aspect ratio γ from 1 to 100. Cells were confined to the x-z plane; hence, Eq. (2) simplifies to $d\theta/dt = \frac{1}{2}(\alpha \sin x \sin z \sin 2\theta - \sin\theta/\Psi - \cos x \cos z)$. We found that including elongation further strengthens the conclusion that gyrotactic motility in vortical flow generates patchiness. While elongation does not affect patch topology for some values of Ψ and Φ, it produces new spatial aggregations for others (Fig. S1 in [13]) and can generate patchiness in some low stability (i.e., large Ψ) regions, where spherical cells remain randomly distributed. Changes in patchiness caused by cell elongation were quantified by calculating $N_E - N$, the difference in N relative to that obtained for spherical cells [Fig. 4(b)]. Out of the 10 values of Ψ and Φ tested, only one gave $N_E \lesssim N$, indicating that cell elongation generally enhances patchiness. A similar conclusion was previously found in the limit of $\Psi = \infty$: cells with larger γ are more likely to escape vortices and aggregate along separatrices [17].

The influence of buoyancy, inertia, and motility on the motion of particles within vortical flows has been studied extensively [9,10,14,17]. Particles that can move only vertically relative to the flow, for example, as a result of buoyancy, correspond to $\Psi = 0$ and cannot generate patchiness in unbounded flows [10]. Particle inertia can in principle induce patchiness [10], but phytoplankton's small size and density contrast ($< 10\%$ denser than seawater) preclude them from aggregating via inertia in most natural flows [18]. In contrast, we have shown that a simple vortical flow can trigger rapid accumulation of gyrotactic phytoplankton over a broad range of parameter space, suggesting that motility plays an important role in determining the spatial distribution of these microorganisms in the environment. Partial support for this hypothesis comes from observations that motile species are more aggregated at small scales than nonmotile species [4,6], though this may be due to alternate mechanisms including chemotaxis [19] and phototaxis [20].

An additional prediction borne out of this model is that different motility characteristics may drive widely different spatial cell distributions. If verified, it would imply that the interaction of motility and flow may control the success of different species in processes like the competition for nutrients and sexual reproduction. One may further speculate that cells could actively control their spatial distribution by adjusting their position in (Φ, Ψ) space (Fig. 2) to favor or prevent aggregation, by either regulating their swimming speed (Φ) or altering their stability (Ψ) via changes in morphology [21], chloroplast position [22], or flagellar stroke [23].

One must, however, be cautious in extending findings from an idealized flow model to realistic flows. While the steady TGV flow is often used as a crude analog for turbulence [10], the latter is time dependent, fully three dimensional, and incorporates a range of scales, including larger-scale fluid motion that can disperse aggregations formed at smaller scales [24]. Therefore, in the same spirit as studies that examined the motion of inertial particles in TGV flow [10], the results presented here open new hypotheses that await to be tested with more realistic flow models (e.g., direct numerical simulation) or in laboratory experiments.

We thank Lyubov Chumakova, Martin Maxey, and Pedro Reis for helpful discussions. This research was funded by a MISTI-France grant to E. C. and R. S. and NSF Grant No. OCE-0744641-CAREER to R. S.

[1] P. Legendre and M.-J. Fortin, Vegetatio **80**, 107 (1989).
[2] J. H. Steele, Nature (London) **248**, 83 (1974).
[3] J. G. Mitchell *et al.*, J. Mar. Syst. **69**, 247 (2008).
[4] S. M. Gallager, H. Yamazaki, and C. S. Davis, Mar. Ecol. Prog. Ser. **267**, 27 (2004).
[5] R. L. Waters, J. G. Mitchell, and J. Seymour, Mar. Ecol. Prog. Ser. **251**, 49 (2003).
[6] L. T. Mouritsen and K. Richardson, J. Plankton Res. **25**, 783 (2003).
[7] W. M. Durham, J. O. Kessler, and R. Stocker, Science **323**, 1067 (2009).
[8] T. J. Pedley and J. O. Kessler, Annu. Rev. Fluid Mech. **24**, 313 (1992).
[9] H. Stommel, J. Mar. Res. **8**, 24 (1949).
[10] M. R. Maxey and S. Corrsin, J. Atmos. Sci. **43**, 1112 (1986).
[11] G. I. Taylor, Philos. Mag. **46**, 671 (1923).
[12] J. O. Kessler, Nature (London) **313**, 218 (1985).
[13] See supplemental material at http://link.aps.org/supplemental/10.1103/PhysRevLett.106.238102 for movies.
[14] J. G. Mitchell, A. Okubo, and J. A. Fuhrman, Limnol. Oceanogr. **35**, 123 (1990).
[15] D. M. Lewis, Proc. R. Soc. A **459**, 1293 (2003).
[16] J. R. Fessler, J. D. Kulick, and J. K. Eaton, Phys. Fluids **6**, 3742 (1994).
[17] C. Torney and Z. Neufeld, Phys. Rev. Lett. **99**, 078101 (2007).
[18] J. Jiménez, Sci. Mar. **61**, 47 (1997).
[19] J. R. Seymour, Marcos, and R. Stocker, Am. Nat. **173**, E15 (2009).
[20] C. Torney and Z. Neufeld, Phys. Rev. Lett. **101**, 078105 (2008).
[21] M. J. Zirbel, F. Veron, and M. I. Latz, J. Phycol. **36**, 46 (2000).
[22] W. Haupt, BioScience **23**, 289 (1973).
[23] M. S. Jones, L. Le Baron, and T. J. Pedley, J. Fluid Mech. **281**, 137 (1994).
[24] L. P. Wang and M. R. Maxey, J. Fluid Mech. **256**, 27 (1993).